Letter

Robust Weak Antilocalization Effect Up to ∼120 K in the van der Waals Crystal $Fe_{5-x}GeTe_2$ with Near-Room-Temperature Ferromagnetism

Zhengxian Li, Deping Guo, Kui Huang, Guodong Ma, Xiaolei Liu, Yueshen Wu, Jian Yuan, Zicheng Tao, Binbin Wang, Xia Wang, Zhiqiang Zou, Na Yu, Geliang Yu, Jiamin Xue, Zhongkai Liu,* Wei Ji,* Jun Li,* and Yanfeng Guo*

Cite This: J. Phys. Chem. Lett. 2023, 14, 5456−5465

Read Online

ACCESS | Metrics & More | Article Recommendations | Supporting Information

ABSTRACT: The van der Waals $Fe_{5-x}GeTe_2$ is a 3d ferromagnetic metal with a high Curie temperature of 275 K. We report herein the observation of an exceptional weak antilocalization (WAL) effect that can persist up to 120 K in an $Fe_{5-x}GeTe_2$ nanoflake, indicating the dual nature with both itinerant and localized magnetism of 3d electrons. The WAL behavior is characterized by the magnetoconductance peak around zero magnetic field and is supported by the calculated localized nondispersive flat band around the Fermi level. The peak to dip crossover starting around 60 K in magnetoconductance is visible, which could be ascribed to temperature-induced changes in Fe magnetic moments and the coupled electronic band structure as revealed by angle-resolved photoemission spectroscopy and first-principles calculations. Our findings would be instructive for understanding the magnetic exchanges in transition metal magnets as well as for the design of next-generation room-temperature spintronic devices.
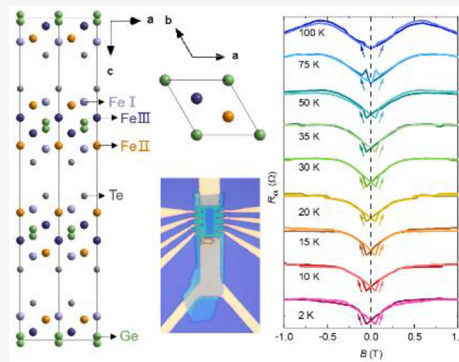
Van der Waals (vdW) bonded magnets have attracted a great deal of attention due to their fundamental and technical merits.[1−6] Their easy exfoliation into multiple or single layers makes them very convenient for the construction of various novel heterostructures and devices. High-Curie temperature (T_C) ferromagnetic (FM) conductors can be used to fabricate magnetic twistronic and spintronic devices and therefore are always being intensely pursued, especially those that can work at room temperature. Fe_nGeTe_2 (n = 3, 4, or 5) ferromagnets with remarkably high T_C values are such model systems. Among the Fe_nGeTe_2 ferromagnets, $Fe_{5-x}GeTe_2$ shows the highest T_C owing to the extra Fe layers that can enhance the strength of FM interactions.[7] Though the Fe_nGeTe_2 magnets are all metals with itinerant electrons, the nature of complicated Fe sites and their exact roles in producing the high-T_C ferromagnetism remain poorly understood.

As a quantum correction to the classical conductivity, the weak antilocalization (WAL) effect can originate from either the strong spin−orbit coupling (SOC) in the bulk materials or spin momentum locking in the topological surface states of topological phases,[8,9] such as in Bi−Se−Te−Sb topological insulators,[10−14] Dirac semimetals with either weak (e.g., graphene) or strong SOC,[15,16] atomic-scale metal films,[17] two-dimensional (2D) transitional metal dichalcogenides (TMDs),[18−21] etc. However, there have been very few reports of the WAL effect in magnetic systems,[22,23] and the WAL effect has not been observed in vdW ferromagnet nanoflakes remains

to the best of our knowledge. In insulating vdW ferromagnets, the ferromagnetism can be described well by an anisotropic Heisenberg model in which local moments correlate with each other via FM interactions,[24,25] while in vdW FM metals such as Fe_3GeTe_2, the electronic itinerancy should be interpreted by using other models. However, the itinerant electron Stoner model seems to be insufficient to account for the magnetism as indicated by the angle-resolved photoemission spectroscopy (ARPES) measurements that unveiled local magnetic moments and heavy Fermion states in Fe_3GeTe_2.[26,27] The result is somewhat exceptional because the WAL effect is inclined to be fully suppressed in transition metal compounds because the strong spin polarization of itinerant electrons can suppress the spin singlet channel that is responsible for the WAL. Considering the dual nature of magnetism in Fe_3GeTe_2, the greater number of Fe sites in $Fe_{5-x}GeTe_2$ naturally offers an excellent opportunity to investigate the WAL effect.
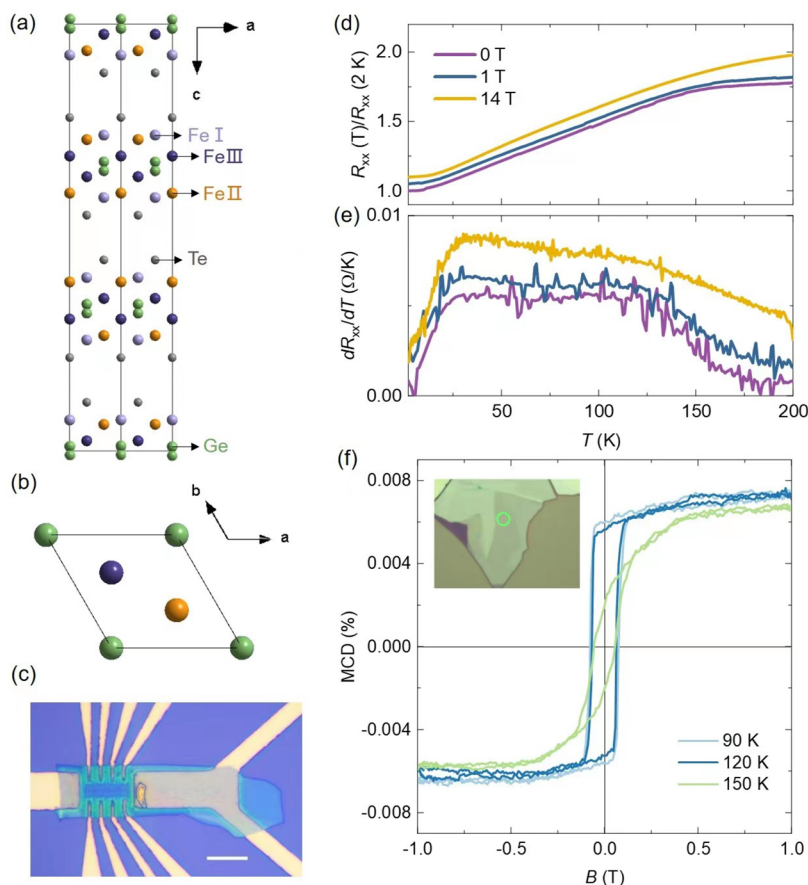
In this work, we performed systematic magnetotransport measurements on $Fe_{5-x}GeTe_2$ crystals. The results unveiled a
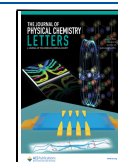
Figure 1. Crystal structure, electrical transport properties, and RMCD measurement results of the few-layer $Fe_{5-x}GeTe_2$. (a and b) Schematic crystal structure of $Fe_{5-x}GeTe_2$ viewed from the b and c axes, respectively. (c) Optical image of a typical device with a Hall bar configuration. (d) $R_{xx}(T)$ under 0, 1, and 14 T perpendicular magnetic fields and (e) the corresponding first derivation. All curves in panels d and e are offset for the sake of clarity. (f) Results measured on the position of the crystal marked by the green circles shown in the inset.

temperature-dependent WAL effect that could persist up to a remarkably high temperature of ~120 K. We also observed a crossover from a peak to dip in the magnetoconductance (MC) around 60 K. Together with our ARPES measurements and first-principles calculations, we proved the results as magnetotransport evidence for the dual nature of both itinerant and localized magnetism in $Fe_{5-x}GeTe_2$.

Panels a and b of Figure 1 depict the schematic crystal structure of $Fe_{5-x}GeTe_2$ viewed from the b and c axes, respectively. The structure consists of eight atom thick monolayers separated by Te atoms among each unit cell. The relatively weak vdW binding force among Te layers facilitates the exfoliation of the crystal into various layers. There are three occupations for Fe in the lattice, namely, Fe I, Fe II, and Fe III. The light purple circles labeled Fe I represent two possible positions of Fe I atoms, which are above or below a given Ge atom, corresponding to two possible Fe−Ge split sites.[7] In $Fe_{5-x}GeTe_2$, the Fe I site is partially occupied and has iron vacancies, while the Fe II and Fe III sites are fully occupied.[28,29] The content of iron vacancies is quantified as ~0.4 with the energy dispersive X-ray spectrum (EDS); i.e., the chemical composition is in fact $Fe_{4.6}GeTe_{2.1}$ when the number of Ge atoms is set to 1 (Figure S1 and Table S1). The specific heat capacity of a $Fe_{5-x}GeTe_2$ bulk crystal shown in Figure S2 reveals an anomaly at 275 K, coinciding with the T_C. Panel c of Figure 1 shows an optical microscope image of the typical structure of our measured device with a 20 μm scale bar, in

which the thickness of the $Fe_{5-x}GeTe_2$ crystal is ~29 nm (10 layers) as confirmed by the atomic force microscopy (AFM) measurement presented in Figure S3. Panels d and e of Figure 1 show the longitudinal resistance (R_{xx}) and its first derivative versus temperature (T), respectively, under out-of-plane external magnetic fields of 0, 1, and 14 T. The data show typical metallic behavior over the measured temperature range and kinks around 120−165 K induced by a possible charge order.[30] The kinks can be significantly suppressed with a large magnetic field of 14 T, while the suppression is nearly negligible at 1 T. When the temperature is decreased to 120 K, the slope of R_{xx} becomes much sharper, which may be closely related to the Fe I moments that start to order at this temperature[31] and are not sensitive to the out-of-plane magnetic field. We also observed a change in the carrier concentration around 125 K, as shown by $R_{xy}(T)$ in Figure S4. Panel f of Figure 1 shows the temperature-dependent reflective magnetic circular dichroism (RMCD) measurements at one position of $Fe_{5-x}GeTe_2$ crystals shown by the optical microscopic image in Figure S5, marked by the green circles, with a sample thickness similar to that in panel c of Figure 1. One can see that the square-shaped hysteresis loops and coercivity at 90 and 120 K are similar, while those at 150 K apparently change, which is an implication of a variation of the spin structure around 120 K. The relatively square hysteresis loops below 120 K indicate the stronger perpendicular magnetic anisotropy;[32] in other words, the magnetic moments
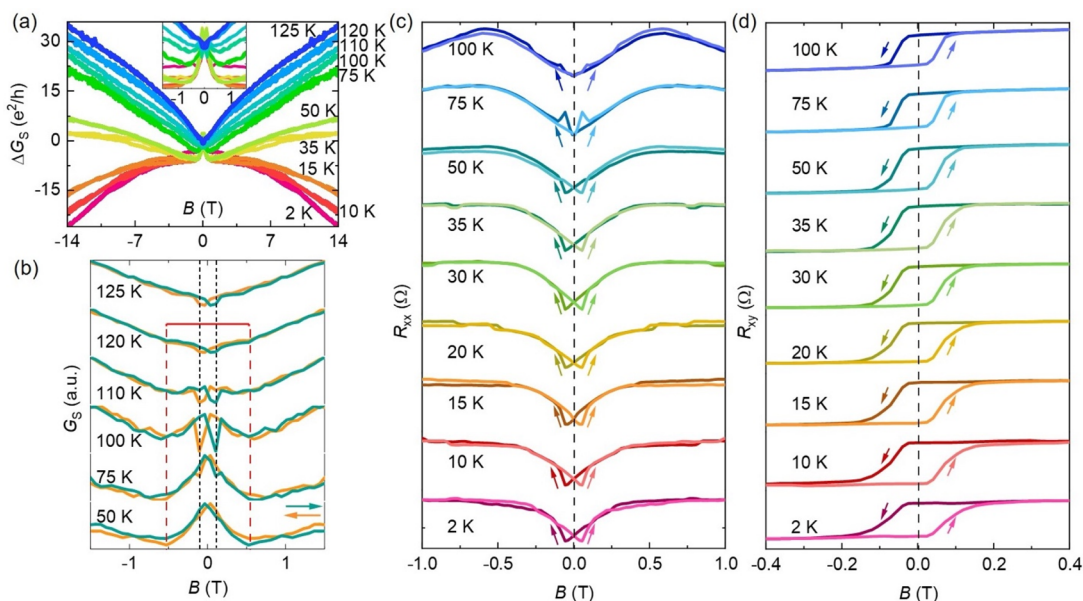
Figure 2. Magnetotransport data of $Fe_{5-x}GeTe_2$. (a) Representative MC curves from 2 to 125 K within the perpendicular sweeping magnetic field range of ±14 T. The inset shows a close-up view of MC at low field showing pronounced WAL cusps. (b) Details of the crossover from peak to dip behavior of the MC. The arrows denote the directions of the sweeping magnetic field. (c) Longitudinal and (d) Hall resistance from 2 to 100 K within the perpendicular sweeping magnetic field range of ±2 T.

can be aligned more easily along the c axis.[33] Above 120 K, the significantly reduced hysteresis loops suggest easier magnetization along the $a-b$ plane.[33] This magnetic anisotropy is closely related with the Fe I moments, which will be discussed below.

Figure 2a depicts the normalized MC of $Fe_{5-x}GeTe_2$ between 2 and 125 K and within the perpendicular sweeping high magnetic field ranging from 0 to ±14 T. The raw data and a detailed explanation of the analysis including symmetrization are shown in Figure S6. Figure 2a shows a transition from negative to positive MC in a wide magnetic field range of 0.5−14 T. From 2 to 15 K, it shows a positive MC, while above 35 K, it becomes a negative MC. The positive MC at high fields above 35 K is commonly observed in ferromagnetic materials because of the suppression of spin scattering by the magnetic field.[34] However, the negative MC at high fields and low temperatures (2−15 K) is likely due to the combination of the supression of magnetic moment fluctuations at low temperatures (for $H = 0$) with the normal resistance increase due to the Lorentz effect.[31] Moreover, the inset of Figure 2a shows a close-up of the low-field data, displaying unusually pronounced MC cusps around zero magnetic field (0−0.5 T), which are characteristic of the WAL effect. With an increase in temperature, the cusps are gradually suppressed. Figure 2b shows the low-field close-up data taken from Figure 2a between 50 and 125 K, showing the evolution of WAL from cusps to dips. The WAL effect starts to change between 50 and 75 K, gradually from the MC peak to dip, as indicated by the black dashed lines. The WAL effect persists up to 120 K, as shown by the low-field peaks, and eventually disappears as the temperature is increased to 125 K, at which point the MC shows only positive behavior, as indicated by the red dashed lines. The arrows denote the directions of the sweeping field. In these plots, the MC ΔG_S is quantified by using a unit of e^2/h, where h is Planck's constant and e is the unit charge.

Despite the fact that the WAL is still visible at 110 and 120 K as indicated by the red dashed lines in Figure 2b, it is too

weak to be well fitted by established models. To improve the quality of the data that could be fitted, we remeasured the longitudinal resistance with a shorter field step from 2 to 100 K at low magnetic fields ranging from 0 to ±2 T, as shown in Figure 2c. Figure 2d presents the corresponding Hall resistance. When $|B| < 0.1$ T, the magnetoresistance (MR) shows a hysteresis that might be caused by the gradual alignment of magnetic domains of Fe ions by the external magnetic field.[35] The dips around zero magnetic field signifying the WAL effect in MR are strikingly displayed. With an increase in temperature, the MR dips become broader. The Hall hysteresis loops show a clear square shape, indicating robust ferromagnetism with strong perpendicular magnetic anisotropy and an anomalous Hall effect. The coercive field (H_c) and the saturation magnetic field (H_m) gradually decrease with an increase in temperature. Compared with those of Fe_3GeTe_2, which is a harder magnetic phase, the coercivity and the shape of the hysteresis loop are smaller and narrower, indicating a weaker perpendicular magnetic anisotropy in $Fe_{5-x}GeTe_2$.[32]

To gain in-depth insights into the WAL effect in $Fe_{5-x}GeTe_2$, a more quantitative analysis of the magnetotransport data is necessary. However, an appropriate theoretical model for describing a ferromagnetic and weakly disordered nanoflake system such as $Fe_{5-x}GeTe_2$ has not been developed yet, so we resorted to nonmagnetic models for the analysis. The limitations of the used models will also be discussed. Generally, the localization effect in a 2D system can be interpreted by the 2D Hikami−Larkin−Nagaoka (HLN) theory.[8] In the regime with a low carrier mobility and strong SOC, the variation of weak field MC is expressed as

$$\Delta G(B) = \frac{\alpha e^2}{2\pi^2 \hbar} \left[\Psi\left(\frac{1}{2} + \frac{\hbar}{4eBl_\varphi^2} \right) - \ln\left(\frac{\hbar}{4eBl_\varphi^2} \right) \right],$$ where B, $\hbar$, Ψ,

and l_φ are the magnetic field, reduced Planck's constant, digamma function, and phase coherence length, respectively. The values of coefficient α should be 1, 0, and $-\frac{1}{2}$ for the
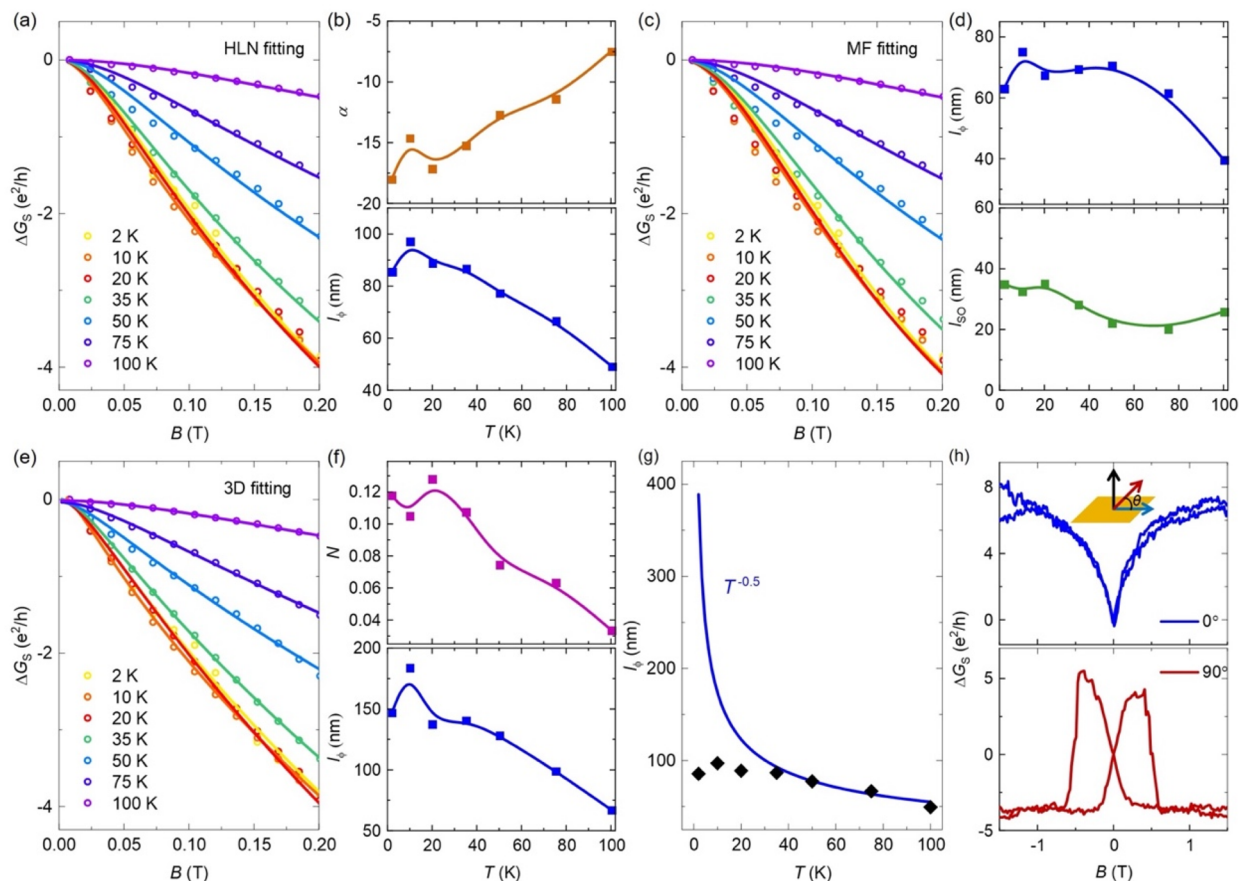
Figure 3. Fitting results of magnetotransport data and angle-dependent MC at low temperatures using different models. (a) Results of HLN fitting (solid lines) to the low-field MC (empty circles) of $Fe_{5−x}GeTe_2$ in the temperature range of 2−100 K. (b) Evolution of coefficient α and phase coherence length l_φ with temperature. Solid lines are visual guides for the data. (c) Fitting curves of MC by using the MF model. (d) Temperature-dependent extracted phase coherence length l_φ and spin−orbit scattering length l_{SO}. Solid lines are visual guides for the data. (e) Results of 3D model fitting to the low-field MC. (f) Temperature-dependent number of quantum channels N and phase coherence length l_φ extracted from the analysis. Solid lines are visual guides for the data. (g) Temperature dependence of phase coherence length l_φ ($\blacklozenge$) extracted from the fits. The solid blue line denotes the results of fitting to $l_\varphi \propto T^{-1/2}$. (h) Angle-dependent MC of a 29 nm thick $Fe_{5−x}GeTe_2$ sample measured at 2 K. The inset of panel h presents the direction of the current (blue arrow) and magnetic field (red arrow) relative to the sample (yellow slab).

orthogonal, unitary, and symplectic cases, respectively.[8] Figure 3a displays the MC between 2 and 100 K denoted by empty circles in the low-magnetic field range, which can be fitted fairly well by using this model indicated by the solid lines. However, considering the presence of hysteresis in MC and to guarantee the authenticity and accuracy of the fit, we fitted only the data between 0 and 0.2 T taken from those in Figure 2c. The fitting results are presented in Figure 3b, yielding the temperature dependence of phase coherence lengths l_φ and coefficients α. The solid lines are the visual guides for the data. It should be noted that the α values are much larger than the theoretically predicted ones for 2D systems, which in fact have no physical meanings, hinting that the WAL effect in $Fe_{5−x}GeTe_2$ is contributed not only from 2D channels but also from other three-dimensional (3D) bulk channels. Such cases were also observed in TI Bi_2Se_3 crystals,[36] $In_xSn_{1−x}Te$ nanoplates,[37] TI $(Bi_{0.57}Sb_{0.43})_2Te_3$ thin films,[38] half-Heusler semiconductor $ScPdBi$,[39] topological semimetal $LuPdBi$,[40] etc. As illustrated in Figure S7, the roughly similar tendency of ρ_{xy}^{AH} and α reveals the close relationship between the magnetization and the WAL effect.[41] As shown in the bottom panel of Figure 3b, the temperature dependence of l_φ indicates the dephasing process due to the enhancement of inelastic scattering by phonons or other electrons with an increase in temperature.

For a 2D disordered electronic system, the field dependence of MC could be calculated by using the Maekawa−Fukuyama (MF) formula expressed as

$$\Delta\sigma(T, B) = \frac{Ne^2}{\pi h}\left\{F\left(\frac{B}{B_\varphi + B_{SO}}\right)\right.$$
$$\left.- \frac{1}{2}\left[F\left(\frac{B}{B_\varphi}\right) - F\left(\frac{B}{B_\varphi + 2B_{SO}}\right)\right]\right\}$$

where $F(z) = \Psi\left(\frac{1}{2} + \frac{1}{z}\right) + \ln(z)$, N is the number of independent conduction channels, $B_\varphi = \hbar/4el_\varphi^2$, and $B_{SO} = \hbar/4el_{SO}^2$, with l_φ and l_{SO} denoting the phase coherence length and spin−orbit scattering length, respectively.[42] The fitting results are presented in Figure 3c as solid lines. The fitting is basically satisfactory except for N values of >20, similar to the case of α. Figure 3d shows the temperature dependence of extracted parameters l_φ and l_{SO}. The solid lines are visual guides for the data. l_φ decreases with an increase in temperature due to the increased inelastic scattering. l_{SO} is relatively independent of T and remains ~30 nm, corresponding to a spin−orbit field B_{SO} of ~0.2 T. Below 100 K, l_φ is
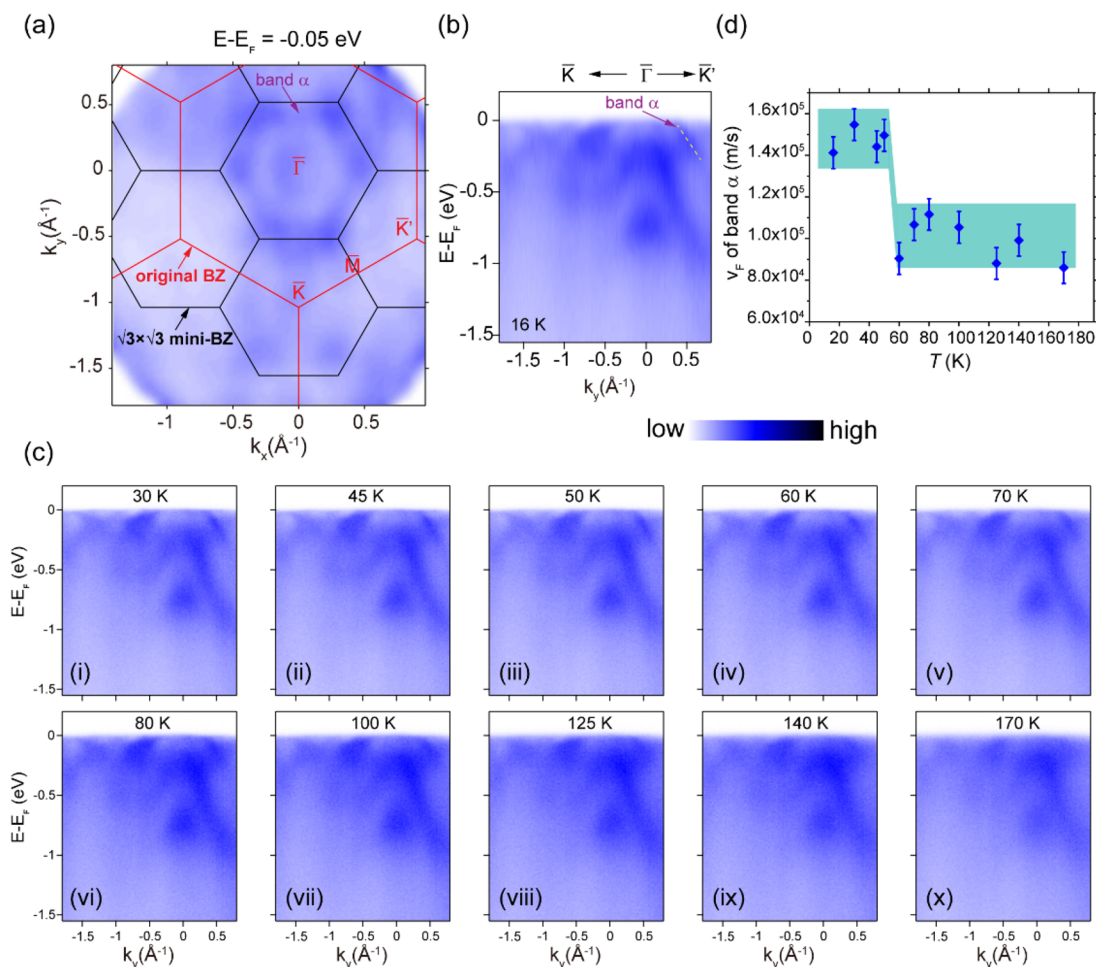
Figure 4. Electronic band structure of $Fe_{5-x}GeTe_2$ measured by ARPES. (a) Photoemission intensity map of constant energy contours in the k_x-k_y plane 0.05 eV below E_F. (b and c) Band dispersions along the high-symmetry $\overline{K}-\overline{\Gamma}-\overline{K}'$ direction with different temperatures. (d) Extracted V_F of band α labeled in panel b, where the error bar corresponds to the energy resolution. The data were collected by using photons for which $h\nu = 112$ eV.

larger than l_{SO}, implying that the spin−orbit scattering is dominated and leads to the negative MC and the WAL effect.

We also examined the 3D model for $Fe_{5-x}GeTe_2$. Figure 3e shows fitting results by using the 3D model expressed as $\Delta\sigma(B) \sim \frac{Ne^2}{4\pi\hbar l_B}\zeta\left(\frac{1}{2}, \frac{1}{2} + \frac{l_B^2}{l_\varphi^2}\right)$, where N is the number of independent interference channels, ζ is the Hurwitz ζ function, and $l_B = \sqrt{\hbar/4eB}$.[16] This equation is an extension of the HLN theory of WL or WAL for the 3D regime at low magnetic fields. The fit based on the 3D model seems more appropriate, but the number of quantum channels extracted from the analysis is too small and decreases with an increase in temperature, as shown in Figure 3f. The solid lines are visual guides for the data. The temperature dependence of phase coherence length l_φ reflects the dephasing due to inelastic scattering as the temperature is increased. In addition, we note that the l_φ values in the 3D model are larger than those in the 2D model. It is clear that for all three models, there is a clear increase in the fitted parameters at 10 K, which may be due to the magnetic order of all Fe moments as indicated by the Mössbauer spectroscopy measurements.[28,31]

As shown in Figure 3a−f, the 2D HLN theory and the 3D models fit the MC data pretty well, but the fit of the MF model is relatively poor. In addition, due to the lack of an accurate

WAL model for describing the FM nanoflake system, the fitting parameters (α and N) are unreasonable, and the dimensionality issue should be further clarified. Among all of the fittings with three models, $T^{-1/2}$ shows the best fit with phase coherence length l_φ in the HLN model. Thus, l_φ values extracted from the HLN fitting (◆) are plotted with temperature in Figure 3g, following an $l_\varphi \propto T^{-1/2}$ ($p = 1$) power law, which suggests a 2D electron−electron interaction dephasing mechanism in our system.[43,44] However, there is a possible saturation of l_φ at lower temperatures, except for a sudden increase at 10 K, which can be attributed to a dephasing from the magnetic spin−spin scattering process or other mechanisms that have been discussed.[43,45,46] Furthermore, the angle-dependent MC measurements on $Fe_{5-x}GeTe_2$ were performed by changing the direction of the applied magnetic field. The data measured at 2 K on an ~29 nm thick sample in Figure 3h display an angle-dependent behavior, strongly implying a basic 2D nature of the electrical transport, because if the WAL effect is mainly in a 3D bulk channel, the MC should be independent of the tilt angles of the magnetic field.[16,40,47] In conclusion, the $T^{-1/2}$ dephasing mechanism and the angle-dependent MC support the basic 2D electrical transport in the 29 nm $Fe_{5-x}GeTe_2$ crystal.

To obtain more information from the electronic band structure of $Fe_{5-x}GeTe_2$, the results of ARPES measurements
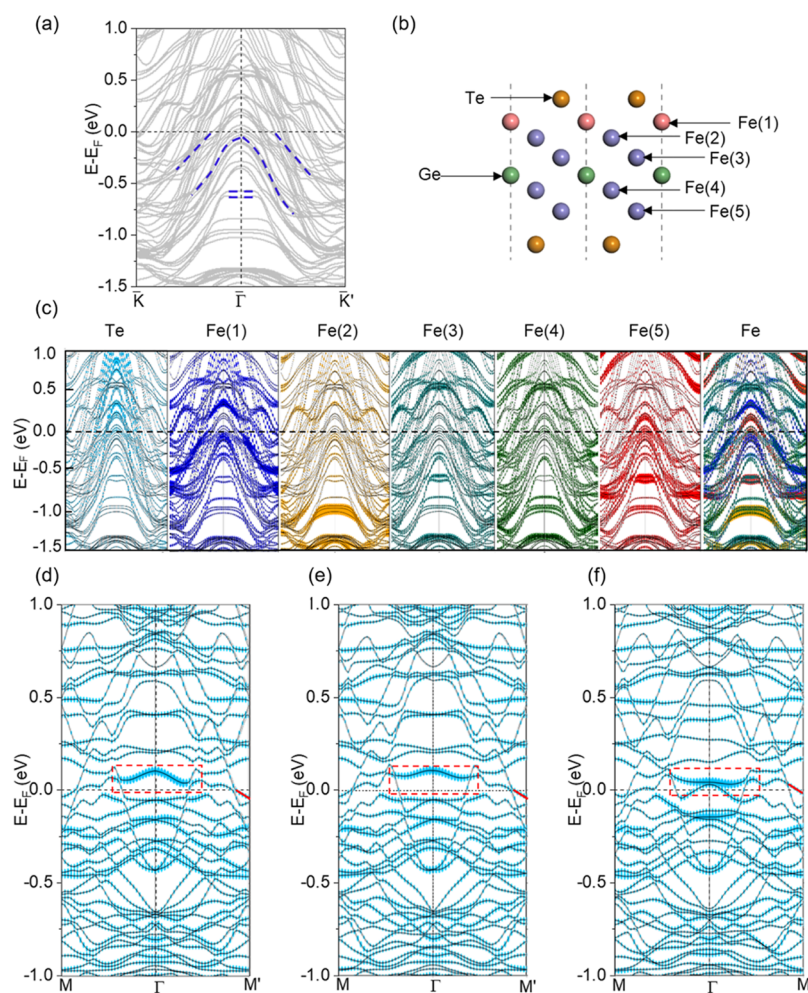
Figure 5. Calculated electronic band structure. (a) Band structure along the high-symmetry $\overline{K}-\overline{\Gamma}-\overline{K}'$ direction in the original Brillouin zone of the bulk crystal. (c) Orbital-resolved band structures of the Te atom and different Fe atoms marked in panel b along the high-symmetry $K-\overline{\Gamma}-\overline{K}'$ direction. Band structure along the high-symmetry $M-\Gamma-M'$ direction in the $\sqrt{3} \times \sqrt{3}$ mini Brillouin zone of the monolayer. (d) Spin orientation along the x axis. (e) Spin orientation along the y axis. (f) Spin orientation along the z axis. The Fermi velocity of the band marked with a red solid line is calculated. The red dotted box marks the obvious different energy bands about the Fermi level in different spin orientations. The blue dots represent the d orbitals of Fe I.

are presented in Figure 4, showing the constant energy contours at the binding energy of 0.05 eV under the $\sqrt{3} \times \sqrt{3}$ reconstruction.[7] The red and black solid lines represent the original and reconstructed Brillouin zones, respectively. Because $Fe_{5-x}GeTe_2$ belongs to space group $R\overline{3}m$, its two adjacent K points are not equivalent, which are distinguished by using $\overline{K}$ and $\overline{K}'$. High-symmetry points $\overline{K}$ and $\overline{K}'$ are also marked in Figure 4a. The band folding between the $\overline{\Gamma}$ and $\overline{K}$ points is clearly seen. From the dispersions along the high-symmetry $K-\Gamma-\overline{K}'$ directions, several hole-like bands could be identified. We focused on one of the hole bands, marked as band α, to monitor its temperature evolution, which is shown in panels b and c of Figure 4. We used a linear function to fit band α at different temperatures and used the slope of the linear function to calculate the Fermi velocity (V_F). The temperature-dependent result is plotted in Figure 4d, which exhibits a sharp jump around 50−60 K, indicating a change in the electronic band structure, specifically, the α band. The change in the other electronic bands near Fermi level E_F is more challenging to analyze. Although the origin of such a change remains unclear, the decrease in the velocity of the hole-type α band at 50−60 K is consistent with the

magnetotransport measurements that show the MC crossover from the peak to dip of the WAL effect as shown in Figure 2b. The ARPES data of band α and its V_F as a function of temperature hint at the close relation between the WAL effect and the electronic structure of $Fe_{5-x}GeTe_2$.

Figure 5a shows the calculated band structure of the bulk sample along the $\overline{K}-\overline{\Gamma}-\overline{K}'$ high-symmetry direction in the original Brillouin zone. The calculations show several hole-like bands around E_F, which are fully consistent with the experimental ones with the intense state being approximately −0.75 eV below E_F. Because Fe I has two positions, the surface Fe atoms are either $Fe(1)$ or $Fe(5)$, as shown in Figure 5b. According to the orbital projection of the band structure presented in Figure 5c, these hole-like bands are mainly derived from the hybrid states of surface $Fe(1)$, $Fe(5)$, and Te atoms, which may be related to the strong influence of $Fe(1)$ and $Fe(5)$ atoms that screen other inner Fe atoms. The intense state approximately −0.75 eV below the hole-like band mainly originates from the d state of the $Fe(5)$ atom. In addition, the electronic structures of in-plane and out-of-plane spin orientations are different around E_F for an $Fe(1)$down− $Fe(1)$up−$Fe(1)$up order of $Fe(1)$ layers (Figure 5d). The

Fermi velocity across the Fermi energy around M′ in the $\sqrt{3} \times \sqrt{3}$ mini-Brillouin zone was calculated. The Fermi velocity of the out-of-plane spin orientation is 1.1×10^5 m/s, while the in-plane spin orientation along the y axis is 0.8×10^5 m/s, which is similar to the sharp jump seen by ARPES measurements. The spin orientation is along the easy magnetization z axis at low temperatures and tends to be aligned along the in-plane direction or to be a helical spin structure due to the complex competition among magnetic anisotropy, Dzyaloshinskii–Moriya interaction, and charge order as the temperature increases.[7] As reported previously, the ordering of the subset Fe(1) layer can give rise to a $\sqrt{3} \times \sqrt{3}$ superstructure on the surface of $Fe_{5-x}GeTe_2$.[7] Moreover, the observed $\sqrt{3} \times \sqrt{3}$ ordering of the Fe(1)–Ge pair breaks the inversion symmetry and consequently leads to antisymmetric DM interaction and hence a commensurate to incommensurate magnetic transition, i.e., a helimagnetic behavior. The competition between helimagnetic behavior and other collinear properties can cause spin reorientation within the temperature ranges of 120–260 and 20–100 K, respectively.[7]

In a magnetic system, the origin of the WAL effect remains controversial, which should be material-specific. It was proved that positive magnetoresistance due to the WAL effect in FM transition metals can be suppressed, such as in Fe and Ni films.[48,49] However, the presence of WAL in other FM systems cannot be completely ruled out due to different relaxation times (τ), spin splitting energies (M), etc. For example, the WAL effect was reported in FM nanostructures,[50] films,[51] and interfaces.[23,52] As opposed to other FM metals, as we mentioned above, the localized nature of partial Fe moments in $Fe_{5-x}GeTe_2$ supports the WAL effect.

Earlier Mössbauer spectroscopy on polycrystalline Fe_5GeTe_2 revealed that the moments on the Fe I sublattice are ordered magnetically below the temperature range of ~100–120 K, while a majority of the Fe moments are ordered at T_C.[31] The observed WAL effect in our experiment emerges at a temperature similar to that at which the Fe I moments are ordered. According to the RMCD data, the hysteresis loop below 120 K is relatively square and strong, which is assumed to be due to the ordered Fe I moments. At a temperature between 120 K and T_C, the hysteresis in RMCD is significantly reduced compared with that at a low temperature, but the hysteresis is still visible because a majority of moments are ordered within this temperature range because the T_C is 275 K. In a similar Mössbauer spectroscopy experiment, it was found that essentially all Fe moments are ordered at 10 K, while approximately 30% of the Fe exhibits a strongly diminished hyperfine field upon warming to 125 K, which is primarily associated with the Fe I sublattice and a portion of Fe III.[28] Furthermore, the magnetic transition at T_C in the polycrystalline sample is associated with Fe II and approximately half of Fe III. The transition in Mössbauer spectra between 70 and 125 K indicates that a large portion of the Fe experiences a collapse in the magnetic hyperfine field of at least 1 order of magnitude, which in combination with the neutron scattering results indicates a remarkably reduced or dynamic magnetic moment. The Mössbauer spectra also witness the structural transition near 100 K through the strong modification of the quadrupole interaction between 70 and 125 K for the Fe I site. Moreover, the Fe I moments cannot be ordered in the temperature range of 100 K to T_C along the c axis because the Fe I moments fluctuate too rapidly in their dynamic model and can generate the exotic domain-wall-(anti)Meron-chain state

that was observed by using Lorentz transmission electron microscopy (LTEM).[33] Below 100 K, the Fe I moments are statically ordered along the c axis and thus could suppress the in-plane magnetization extinguishing the (anti)Meron chains and merging into the continuous domain wall.[28,33]

The evolution of the spin structure of $Fe_{5-x}GeTe_2$, as indicated via combination with the Mössbauer spectroscopy,[28,31] LTEM, RMCD, ARPES, and magnetotransport measurements, could be summarized in several steps. From a low temperature to 60–70 K, essentially all Fe moments are ordered; from 60–70 to 100–125 K, primarily the Fe I sublattice and a portion of Fe III moments experience a collapse, and then from 100–125 K to T_C, the Fe II and approximately half of the Fe III moments are ordered. The results indicate that the WAL effect is closely related with the Fe I moments in $Fe_{5-x}GeTe_2$.

In conclusion, we observed a WAL effect in $Fe_{5-x}GeTe_2$ nanoflakes that can persist up to 120 K. When we fit the experimental data with the HLN, MF, 3D models, and measuring angle-dependent magnetotransport, the WAL effect in a 29 nm thick $Fe_{5-x}GeTe_2$ crystal shows a 2D feature. Additionally, we further studied the WAL behavior of $Fe_{5-x}GeTe_2$ in more detail through RMCD, ARPES, and first-principles calculations, which unveil that the crossover of dip to peak behavior in magnetoresistance could be attributed to a temperature-induced spin reorientation and variation of Fe magnetic moments. Our observation of the WAL effect in the $Fe_{5-x}GeTe_2$ crystal provides evidence for the dual nature of Fe moments, which shed light on the correlation between the electronic structure and magnetism in this family of magnets.

■ ASSOCIATED CONTENT

Data Availability Statement

The data that support the findings of this study are available from the corresponding authors upon reasonable request.

ⓢ Supporting Information

The Supporting Information is available free of charge at https://pubs.acs.org/doi/10.1021/acs.jpclett.3c00380.

> Results of the EDS measurements, specific heat capacity of the bulk $Fe_{5-x}GeTe_2$ crystal, AFM measurement, temperature-dependent Hall resistance R_{xy}, RMCD measurements, raw data of magnetoresistance, and temperature dependent-anomalous Hall and α coefficients (PDF)

■ AUTHOR INFORMATION

Corresponding Authors

Yanfeng Guo — *School of Physical Science and Technology, ShanghaiTech University, Shanghai 201210, China; ShanghaiTech Laboratory for Topological Physics, Shanghai 201210, China;* ⓞ orcid.org/0000-0002-9386-4857; Email: guoyf@shanghaitech.edu.cn

Wei Ji — *Department of Physics and Beijing Key Laboratory of Optoelectronic Functional Materials & Micro-nano Devices, Renmin University of China, Beijing 100190, China;* ⓞ orcid.org/0000-0001-5249-6624; Email: wji@ruc.edu.cn

Jun Li — *School of Physical Science and Technology, ShanghaiTech University, Shanghai 201210, China; ShanghaiTech Laboratory for Topological Physics, Shanghai 201210, China;* Email: lijun3@shanghaitech.edu.cn

Zhongkai Liu − *School of Physical Science and Technology, ShanghaiTech University, Shanghai 201210, China; ShanghaiTech Laboratory for Topological Physics, Shanghai 201210, China*; Email: liuzhk@@shanghaitech.edu.cn

Authors

Zhengxian Li − *School of Physical Science and Technology, ShanghaiTech University, Shanghai 201210, China;*
 ⊚ orcid.org/0000-0002-5292-8914

Deping Guo − *Department of Physics and Beijing Key Laboratory of Optoelectronic Functional Materials & Micronano Devices, Renmin University of China, Beijing 100190, China*

Kui Huang − *School of Physical Science and Technology, ShanghaiTech University, Shanghai 201210, China*

Guodong Ma − *National Laboratory of Solid State Microstructures and School of Physics, Nanjing University, Nanjing 210093, China*

Xiaolei Liu − *School of Physical Science and Technology, ShanghaiTech University, Shanghai 201210, China;*
 ⊚ orcid.org/0000-0001-9590-9003

Yueshen Wu − *School of Physical Science and Technology, ShanghaiTech University, Shanghai 201210, China*

Jian Yuan − *School of Physical Science and Technology, ShanghaiTech University, Shanghai 201210, China*

Zicheng Tao − *School of Physical Science and Technology, ShanghaiTech University, Shanghai 201210, China*

Binbin Wang − *School of Physical Science and Technology, ShanghaiTech University, Shanghai 201210, China*

Xia Wang − *School of Physical Science and Technology and Analytical Instrumentation Center, School of Physical Science and Technology, ShanghaiTech University, Shanghai 201210, China*

Zhiqiang Zou − *School of Physical Science and Technology and Analytical Instrumentation Center, School of Physical Science and Technology, ShanghaiTech University, Shanghai 201210, China*

Na Yu − *School of Physical Science and Technology and Analytical Instrumentation Center, School of Physical Science and Technology, ShanghaiTech University, Shanghai 201210, China*

Geliang Yu − *National Laboratory of Solid State Microstructures and School of Physics, Nanjing University, Nanjing 210093, China*

Jiamin Xue − *School of Physical Science and Technology, ShanghaiTech University, Shanghai 201210, China;*
 ⊚ orcid.org/0000-0002-1892-1743

Complete contact information is available at:
https://pubs.acs.org/10.1021/acs.jpclett.3c00380

Author Contributions

Z. Li and D.G. contributed equally to this work. Y.G. conceived the project. Z. Li grew the crystals, performed the basic characterizations, fabricated the devices, and measured the magnetotransport properties with the help of Z.T., J.Y., X.L., X.W., Z.Z., N.Y., B.W., and Y.W. directed by J.X., Y.G., and J.L. K.H. performed the ARPES measurements directed by Z. Liu. D.G. performed the calculations directed by W.J. G.M. measured the RMCD directed by G.Y. All authors contributed to the writing of the manuscript.

Notes

The authors declare no competing financial interest.

REFERENCES

(1) Novoselov, K. S.; Geim, A. K.; Morozov, S. V.; Jiang, D.-e.; Zhang, Y.; Dubonos, S. V.; Grigorieva, I. V.; Firsov, A. A. Electric field effect in atomically thin carbon films. *Science* **2004**, *306*, 666−669.

(2) Zhang, Y.; Tan, Y.-W.; Stormer, H. L.; Kim, P. Experimental observation of the quantum Hall effect and Berry's phase in graphene. *Nature* **2005**, *438*, 201−204.

(3) Mak, K. F.; Lee, C.; Hone, J.; Shan, J.; Heinz, T. F. Atomically thin MoS_2: a new direct-gap semiconductor. *Phys. Rev. Lett.* **2010**, *105*, 136805.

(4) Lu, J.; Zheliuk, O.; Leermakers, I.; Yuan, N. F.; Zeitler, U.; Law, K. T.; Ye, J. Evidence for two-dimensional Ising superconductivity in gated MoS_2. *Science* **2015**, *350*, 1353−1357.

(5) Xi, X.; Zhao, L.; Wang, Z.; Berger, H.; Forró, L.; Shan, J.; Mak, K. F. Strongly enhanced charge-density-wave order in monolayer $NbSe_2$. *Nat. Nanotechnol.* **2015**, *10*, 765−769.

(6) Li, L.; O'Farrell, E.; Loh, K.; Eda, G.; Özyilmaz, B.; Castro Neto, A. H. Controlling many-body states by the electric-field effect in a two-dimensional material. *Nature* **2016**, *529*, 185−189.

(7) Ly, T. T.; Park, J.; Kim, K.; Ahn, H.-B.; Lee, N. J.; Kim, K.; Park, T.-E.; Duvjir, G.; Lam, N. H.; Jang, K.; et al. Direct observation of Fe-Ge ordering in $Fe_{5−x}GeTe_2$ crystals and resultant helimagnetism. *Adv. Funct. Mater.* **2021**, *31*, 2009758.

(8) Hikami, S.; Larkin, A. I.; Nagaoka, Y. Spin-orbit interaction and magnetoresistance in the two dimensional random system. *Prog. Theor. Phys.* **1980**, *63*, 707−710.

(9) Nomura, K.; Koshino, M.; Ryu, S. Topological delocalization of two-dimensional massless Dirac fermions. *Phys. Rev. Lett.* **2007**, *99*, 146806.

(10) Cha, J. J.; Kong, D.; Hong, S.-S.; Analytis, J. G.; Lai, K.; Cui, Y. Weak antilocalization in $Bi_2(Se_xTe_{1−x})_3$ nanoribbons and nanoplates. *Nano Lett.* **2012**, *12*, 1107−1111.

(11) Bao, L.; He, L.; Meyer, N.; Kou, X.; Zhang, P.; Chen, Z.-g.; Fedorov, A. V.; Zou, J.; Riedemann, T. M.; Lograsso, T. A.; et al. Weak anti-localization and quantum oscillations of surface states in topological insulator Bi_2Se_2Te. *Sci. Rep.* **2012**, *2*, 726.

(12) Chen, J.; Qin, H.; Yang, F.; Liu, J.; Guan, T.; Qu, F.; Zhang, G.; Shi, J.; Xie, X.; Yang, C.; et al. Gate-voltage control of chemical potential and weak antilocalization in Bi_2Se_3. *Phys. Rev. Lett.* **2010**, *105*, 176602.

(13) He, H.-T.; Wang, G.; Zhang, T.; Sou, I.-K.; Wong, G. K.; Wang, J.-N.; Lu, H.-Z.; Shen, S.-Q.; Zhang, F.-C. Impurity effect on weak

antilocalization in the topological insulator Bi_2Te_3. *Phys. Rev. Lett.* **2011**, *106*, 166805.

(14) Li, H.; Wang, H.-W.; Li, Y.; Zhang, H.; Zhang, S.; Pan, X.-C.; Jia, B.; Song, F.; Wang, J. Quantitative analysis of weak antilocalization effect of topological surface states in topological insulator $BiSbTeSe_2$. *Nano Lett.* **2019**, *19*, 2450−2455.

(15) Tikhonenko, F. V.; Kozikov, A. A.; Savchenko, A. K.; Gorbachev, R. V. Transition between electron localization and antilocalization in graphene. *Phys. Rev. Lett.* **2009**, *103*, 226801.

(16) Nakamura, H.; Huang, D.; Merz, J.; Khalaf, E.; Ostrovsky, P.; Yaresko, A.; Samal, D.; Takagi, H. Robust weak antilocalization due to spin-orbital entanglement in Dirac material Sr_3SnO. *Nat. Commun.* **2020**, *11*, 1161.

(17) Matetskiy, A. V.; Denisov, N. V.; Zotov, A. V.; Saranin, A. A. Weak antilocalization at the atomic-scale limit of metal film thickness. *Nano Lett.* **2019**, *19*, 570−575.

(18) Liu, H.; Bao, L.; Zhou, Z.; Che, B.; Zhang, R.; Bian, C.; Ma, R.; Wu, L.; Yang, H.; Li, J.; et al. Quasi-2D transport and weak antilocalization effect in few-layered VSe_2. *Nano Lett.* **2019**, *19*, 4551−4559.

(19) Naylor, C. H.; Parkin, W. M.; Ping, J.; Gao, Z.; Zhou, Y. R.; Kim, Y.; Streller, F.; Carpick, R. W.; Rappe, A. M.; Drndic, M.; et al. Monolayer single-crystal 1T'-$MoTe_2$ grown by chemical vapor deposition exhibits weak antilocalization effect. *Nano Lett.* **2016**, *16*, 4297−4304.

(20) Schmidt, H.; Yudhistira, I.; Chu, L.; Castro Neto, A. H.; Ozyilmaz, B.; Adam, S.; Eda, G. Quantum transport and observation of Dyakonov-Perel spin-orbit scattering in monolayer MoS_2. *Phys. Rev. Lett.* **2016**, *116*, 046803.

(21) Wu, Y.; Xing, H.; Lian, C.-S.; Lian, H.; He, J.; Duan, W.; Liu, J.; Mao, Z.; Liu, Y. Ion intercalation engineering of electronic properties of two-dimensional crystals of 2H−$TaSe_2$. *Phys. Rev. Mater.* **2019**, *3*, 104003.

(22) Cai, X.; Yue, J.; Xu, P.; Jalan, B.; Pribiag, V. S. From weak antilocalization to Kondo scattering in a magnetic complex oxide interface. *Phys. Rev. B* **2021**, *103*, 115434.

(23) Cai, X.; Ayino, Y.; Yue, J.; Xu, P.; Jalan, B.; Pribiag, V. S. Disentangling spin-orbit coupling and local magnetism in a quasi-two-dimensional electron system. *Phys. Rev. B* **2019**, *100*, 081402.

(24) Gong, C.; Li, L.; Li, Z.; Ji, H.; Stern, A.; Xia, Y.; Cao, T.; Bao, W.; Wang, C.; Wang, Y.; et al. Discovery of intrinsic ferromagnetism in two-dimensional van der Waals crystals. *Nature* **2017**, *546*, 265−269.

(25) Huang, B.; Clark, G.; Navarro-Moratalla, E.; Klein, D. R.; Cheng, R.; Seyler, K. L.; Zhong, D.; Schmidgall, E.; McGuire, M. A.; Cobden, D. H.; et al. Layer-dependent ferromagnetism in a van der Waals crystal down to the monolayer limit. *Nature* **2017**, *546*, 270−273.

(26) Zhang, Y.; Lu, H.; Zhu, X.; Tan, S.; Feng, W.; Liu, Q.; Zhang, W.; Chen, Q.; Liu, Y.; Luo, X.; et al. Emergence of Kondo lattice behavior in a van der Waals itinerant ferromagnet, Fe_3GeTe_2. *Sci. Adv.* **2018**, *4*, eaao6791.

(27) Xu, X.; Li, Y. W.; Duan, S. R.; Zhang, S. L.; Chen, Y. J.; Kang, L.; Liang, A. J.; Chen, C.; Xia, W.; Xu, Y.; et al. Signature for non-Stoner ferromagnetism in the van der Waals ferromagnet Fe_3GeTe_2. *Phys. Rev. B* **2020**, *101*, 201104.

(28) May, A. F.; Ovchinnikov, D.; Zheng, Q.; Hermann, R.; Calder, S.; Huang, B.; Fei, Z.; Liu, Y.; Xu, X.; McGuire, M. A. Ferromagnetism near room temperature in the cleavable van der Waals crystal Fe_5GeTe_2. *ACS Nano* **2019**, *13*, 4436−4442.

(29) Stahl, J.; Shlaen, E.; Johrendt, D. The van der Waals ferromagnets $Fe_{5-\delta}GeTe_2$ and $Fe_{5-\delta-x}Ni_xGeTe_2$ - crystal structure, stacking faults, and magnetic properties. *Z. anorg. allg. Chem.* **2018**, *644*, 1923−1929.

(30) Wu, X.; Lei, L.; Yin, Q.; Zhao, N.-N.; Li, M.; Wang, Z.; Liu, Q.; Song, W.; Ma, H.; Ding, P.; et al. Direct observation of competition between charge order and itinerant ferromagnetism in the van der Waals crystal $Fe_{5-x}GeTe_2$. *Phys. Rev. B* **2021**, *104*, 165101.

(31) May, A. F.; Bridges, C. A.; McGuire, M. A. Physical properties and thermal stability of $Fe_{5-x}GeTe_2$ single crystals. *Phys. Rev. Mater.* **2019**, *3*, 104401.

(32) Tan, C.; Lee, J.; Jung, S. G.; Park, T.; Albarakati, S.; Partridge, J.; Field, M. R.; McCulloch, D. G.; Wang, L.; Lee, C. Hard magnetic properties in nanoflake van der Waals Fe_3GeTe_2. *Nat. Commun.* **2018**, *9*, 1554.

(33) Gao, Y.; Yin, Q.; Wang, Q.; Li, Z.; Cai, J.; Zhao, T.; Lei, H.; Wang, S.; Zhang, Y.; Shen, B. Spontaneous (anti) Meron chains in the domain walls of van der Waals ferromagnetic $Fe_{5-x}GeTe_2$. *Adv. Mater.* **2020**, *32*, 2005228.

(34) Yamada, H.; Takada, S. Negative magnetoresistance of ferromagnetic metals due to spin fluctuations. *Prog. Theor. Phys.* **1972**, *48*, 1828−1848.

(35) Chiu, S.-P.; Yamanouchi, M.; Oyamada, T.; Ohta, H.; Lin, J.-J. Gate tunable spin-orbit coupling and weak antilocalization effect in an epitaxial $La_{2/3}Sr_{1/3}MnO_3$ thin film. *Phys. Rev. B* **2017**, *96*, 085143.

(36) Checkelsky, J. G.; Hor, Y. S.; Liu, M. H.; Qu, D. X.; Cava, R. J.; Ong, N. P. Quantum interference in macroscopic crystals of nonmetallic Bi_2Se_3. *Phys. Rev. Lett.* **2009**, *103*, 246601.

(37) Shen, J.; Xie, Y.; Cha, J. J. Revealing surface states in In-doped SnTe nanoplates with low bulk mobility. *Nano Lett.* **2015**, *15*, 3827−3832.

(38) Lang, M.; He, L.; Kou, X.; Upadhyaya, P.; Fan, Y.; Chu, H.; Jiang, Y.; Bardarson, J. H.; Jiang, W.; Choi, E. S.; et al. Competing weak localization and weak antilocalization in ultrathin topological insulators. *Nano Lett.* **2013**, *13*, 48−53.

(39) Zhang, J.; Hou, Z.; Zhang, C.; Chen, J.; Li, P.; Wen, Y.; Zhang, Q.; Wang, W.; Zhang, X. Weak antilocalization effect and high-pressure transport properties of ScPdBi single crystal. *Appl. Phys. Lett.* **2019**, *115*, 172407.

(40) Xu, G.; Wang, W.; Zhang, X.; Du, Y.; Liu, E.; Wang, S.; Wu, G.; Liu, Z.; Zhang, X. X. Weak antilocalization effect and non-centrosymmetric superconductivity in a topologically nontrivial semimetal LuPdBi. *Sci. Rep.* **2014**, *4*, 5709.

(41) Liu, M.; Zhang, J.; Chang, C. Z.; Zhang, Z.; Feng, X.; Li, K.; He, K.; Wang, L. L.; Chen, X.; Dai, X.; et al. Crossover between weak antilocalization and weak localization in a magnetically doped topological insulator. *Phys. Rev. Lett.* **2012**, *108*, 036805.

(42) Maekawa, S.; Fukuyama, H. Magnetoresistance in two-dimensional disordered systems: effects of Zeeman splitting and spin-orbit scattering. *J. Phys. Soc. Jpn.* **1981**, *50*, 2516−2524.

(43) Lin, J. J.; Bird, J. P. Recent experimental studies of electron dephasing in metal and semiconductor mesoscopic structures. *J. Phys.: Condens. Matter* **2002**, *14*, R501−R596.

(44) Lee, P. A.; Ramakrishnan, T. V. Disordered electronic systems. *Rev. Mod. Phys.* **1985**, *57*, 287−337.

(45) Kaminski, A.; Glazman, L. I. Electron energy relaxation in the presence of magnetic impurities. *Phys. Rev. Lett.* **2001**, *86*, 2400−2403.

(46) Engels, S.; Terrés, B.; Epping, A.; Khodkov, T.; Watanabe, K.; Taniguchi, T.; Beschoten, B.; Stampfer, C. Limitations to carrier mobility and phase-coherent transport in bilayer graphene. *Phys. Rev. Lett.* **2014**, *113*, 126801.

(47) Stephen, G. M.; Vail, O. A.; Lu, J.; Beck, W. A.; Taylor, P. J.; Friedman, A. L. Weak antilocalization and anisotropic magneto-resistance as a probe of surface states in topological $Bi_2Te_xSe_{3-x}$ thin films. *Sci. Rep.* **2020**, *10*, 4845.

(48) Dugaev, V. K.; Bruno, P.; Barnaś, J. Weak localization in ferromagnets with spin-orbit interaction. *Phys. Rev. B* **2001**, *64*, 144423.

(49) Kurzweil, N.; Kogan, E.; Frydman, A. Absence of weak antilocalization in ferromagnetic films. *Phys. Rev. B* **2010**, *82*, 235104.

(50) Neumaier, D.; Wagner, K.; Geißler, S.; Wurstbauer, U.; Sadowski, J.; Wegscheider, W.; Weiss, D. Weak localization in ferromagnetic (Ga,Mn)As nanostructures. *Phys. Rev. Lett.* **2007**, *99*, 116803.

(51) Gupta, S.; Sachan, R.; Narayan, J. Evidence of weak antilocalization in epitaxial TiN thin films. *J. Magn. Magn. Mater.* **2020**, *498*, 166094.

(52) Stornaiuolo, D.; Jouault, B.; Di Gennaro, E.; Sambri, A.; D'Antuono, M.; Massarotti, D.; Granozio, F. M.; Di Capua, R.; De Luca, G. M.; Pepe, G. P.; et al. Interplay between spin-orbit coupling and ferromagnetism in magnetotransport properties of a spin-polarized oxide two-dimensional electron system. *Phys. Rev. B* **2018**, *98*, 075409.

(53) Bao, S.; Wang, W.; Shangguan, Y.; Cai, Z.; Dong, Z.-Y.; Huang, Z.; Si, W.; Ma, Z.; Kajimoto, R.; Ikeuchi, K.; et al. Neutron spectroscopy evidence on the dual nature of magnetic excitations in a van der Waals metallic ferromagnet $Fe_{2.72}GeTe_2$. *Phys. Rev. X* **2022**, *12*, 011022.

■ NOTE ADDED IN PROOF

When we prepared our manuscript, we became aware of recent inelastic neutron scattering measurements of $Fe_{2.72}GeTe_2$, which supported direct evidence for the coexistence of both local moments and itinerant electrons and the Kondo effect between them.[53]